W02

Proceedings of the 5th International Conference on Inverse Problems in Engineering: Theory and Practice, Cambridge, UK, 11-15th July 2005

STATE-SPACE REPRESENTATION OF CLOSED CONTOURS IN ELECTRICAL CAPACITANCE TOMOGRAPHY

D. WATZENIG, M. BRANDNER, G. STEINER and B. BRANDSTÄTTER
Christian Doppler Laboratory for Automotive Measurement Research located at the Institute of Electrical Measurement and Measurement Signal Processing, Graz University of Technology, Kopernikusgasse 24, 8010 Graz, Austria
e-mail: {watzenig, brandner, steiner}@emt.tugraz.at, brand@ieee.org

Abstract - In Electrical Capacitance Tomography (ECT) the main focus is on the reconstruction of distinct objects with sharp transitions between the phases. Being inherently ill-posed, the reconstruction algorithm requires some sort of regularization to stabilize the solution of the inverse problem. However, introducing regularization may counteract the reconstruction of well-defined contours for grid-based methods. Level set propagation approaches able to model sharp phase boundaries suffer from high computational demands. In this contribution two different state-space representations of closed contours based on B-Splines and on Fourier descriptors are investigated. Both approaches allow to describe the problem with only a small set of state-space variables. Regularization is incorporated implicitly which can be directly interpreted in the object domain as it relates to smooth contours. To solve the inverse problem, statistical inversion is performed by means of particle filtering providing the opportunity to incorporate prior information conveniently and to take measurement uncertainties into account.

1. INTRODUCTION

Electrical Capacitance Tomography (ECT) is a non-invasive image-based technique that aims at estimating the permittivity distribution (ε_r-distribution) within closed objects [14]. Such objects are, for instance, pipelines in the oil industry or chambers and vessels in the food industry. Voltage patterns are applied to the electrodes which are mounted along the circumference. The resulting potentials which depend on the materials inside the closed object are measured. Based on these measurements, the spatial material distribution is reconstructed. However, this reconstruction task is a nonlinear and severely ill-posed inverse problem. A lot of different algorithms have been developed and applied to tomographic tasks for two-phase flow fields in recent years with the objective to improve the image quality and to reduce the computational effort in order to approach real-time. Finite Element Methods (FEM) which are widely in use are not well suited when the reconstruction of phase boundaries is of interest due to the need of regularization. Regularization simply incorporates some a priori assumption on the material distribution and is done by adding a regularization term to the original functional to be minimized. The amount of regularization is crucial for the reconstruction task and, therefore, many different approaches have been proposed [4]. But up to now there is no universally valid rule to adjust this parameter. Another drawback of regularization for grid-based methods is that it causes a blurring of object interfaces. However, in process tomography the main focus is on the identification of distinct objects with sharp boundaries (e.g. gas bubbles in oil). To overcome the problem of blurred images, different edge preserving methods for finite element based reconstruction techniques have been introduced. For example, the use of an auxiliary variable permits to linearize the problem and to derive a deterministic algorithm based on alternate minimizations [7]. Due to the increased computational effort, this method is not applicable for real-time requirements. To overcome this drawback in case of a two-phase field, various mesh grouping methods have been proposed (see e.g. [6]). The main disadvantage is that they rely on threshold levels which have to be found out by trial and error. A different possibility is to use the Boundary Element Method (BEM) instead of FEM. The inverse problem can then be solved e.g. by applying a numerical level set propagation approach [8]. The method inherently preserves object edges and implements a regularization based on the smoothness of the level set function. However, the drawback is the computational complexity due to a large number of parameters. To achieve sharp edges without increased computational effort it is reasonable to describe material boundaries by means of a parameterized curves. Possible methods to represent the boundary of an object are the use of active contours [2] or the application of Fourier descriptors [11]. They are especially suitable for dynamic problems such as streaming fluids. Both methods use low order state-space representations to incorporate model-based information into a boundary finding process for continuously deformable objects. Object tracking and solving the inverse ECT problem can be performed by matching the parameters with regard to a minimum error between measured and predicted potentials. The inverse problem can be solved, for instance, in a least squares sense.

In a scenario where noise sources can be identified and modeled the reconstruction of unknown objects given uncertain information can be formulated as statistical inference problem. A popular framework to incorporate

stochastic state transistions and measurements originate from the Bayes rule. One algorithm based on this principle is the Kalman Filter (KF). In order to deal with the inherent non-linearity of the measurement equations within the ECT framework, the Extended Kalman Filter (EKF) has been applied to tomographic tasks [12, 13]. Its applicability is subjected to state vectors that are random Gaussian variables. In addition the occurance of multiple object hypotheses – as frequently encountered during the reconstruction of dynamical setups – can not be properly tackled by an algorithm restricted to unimodal Gaussian state vectors. A less restrictive formulation of the Bayes principle based on Monte Carlo (MC) simulations and a numerical approximation of non-Gaussian state densities is given by the family of Particle Filters (PFs). In a direct comparison to the EKF the PF offers the possibility of a non-approximate evaluation of the state transitions – even in the non-linear case – and multimodal state densities. Another appealing property of PF is their straightforward incorporation of a priori information about the inner state of a dynamic system. On the downside these advantages come at the cost of additional computations spent in the density approximation and the management of samples in state space. PF have already been applied to inverse problems in tomographic applications [5, 9] but so far the state space of these reported approaches was setup based on the set of finite elements used in the reconstruction step. The resulting state vectors are large which directly impacts the computational costs and real-time performance of the algorithms. The use of low order state space representations of closed contours enables the application of PF with considerably reduced computational effort.

The remainder of this paper is structured as follows: Section 2 briefly describes the solution of the forward problem with BEM. The representation of closed contours in state-space by B-Splines and Fourier descriptors is addressed in Section 3 followed by an introduction of the applied PF in Section 4. The proposed contour models are used for the reconstruction of two-phase test distributions and compared regarding the achievable reconstruction performance in Section 5.

2. SOLUTION OF THE FORWARD PROBLEM

In ECT, the forward problem consists of determining the distribution of the electric scalar potential u_p for the active electrode pattern p and subsequently the electric field strength and the capacitance for a given permittivity distribution within the pipe. In each cycle of the applied electrode pattern, two electrodes are active, i.e. a certain potential is prescribed, while the remaining electrodes are the measurement electrodes. The governing equation is a Laplace equation with Dirichlet boundary conditions.

$$\nabla \cdot (\varepsilon \nabla u_p) = 0 \tag{1}$$

$$u_p\big|_{\Gamma_0} = u_{0,p} \tag{2}$$

where Γ_0 are the boundaries, where Dirichlet boundary conditions are prescribed. In the present work, the simulation environment consists of a tube where 16 electrodes are placed equidistantly around the circumference and a conductive shield at ground potential at some distance from the tube (Figure 1(a)).

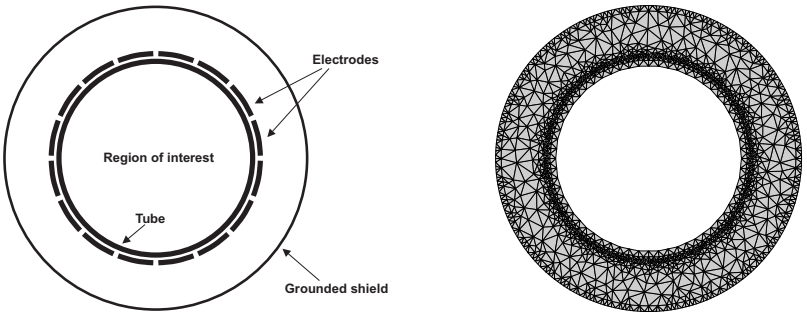

(a) Cross-section of the used ECT sensor. (b) Discretization of the pipe.

Figure 1: Cross-section of the ECT sensor with 16 electrodes mounted on a pipe. The outer space is circumvented by a grounded conductive shielding. On the right, the discretization into linear finite elements of the electrodes, the tube and the outer space is depicted. Object boundaries in the region of interest are described by boundary elements.

As neither the geometry nor the material values between the tube and the grounded shield change, it is advantageous to discretize the Laplace equation in this region with finite elements, whereas due to changing geometries and material values in the interior of the pipe, the BEM is applied [8]. Using the BEM in the region of interest increases the spatial resolution, since the discretization error due to finite elements is avoided. Figure 1(b) illus-

trates the discretization of the electrodes, the tube and the outer space with linear triangular finite elements while the interior of the pipe is one region for the BEM.

3. REPRESENTATION OF CLOSED CONTOURS IN STATE-SPACE

Contours can be described as the boundaries between distinct regions with different properties. In the case of ECT, regions are distinguished by their distinct permittivity values. The contour $\mathcal{C}$ in $\mathbb{R}^2$ can be described by means of a vector-valued function $\mathbb{R} \rightarrow \mathbb{R} \times \mathbb{R} : s \mapsto \mathbf{c}(s)$ parameterized by $s \in [0, 1]$. $\mathcal{C}$ is *closed* if and only if $\mathbf{c}(0) = \mathbf{c}(1)$ and the Cartesian coordinates (x, y) of a point on the contour are given by the elements of $\mathbf{c}(s)$ as $\mathbf{c}(s) = (x(s), y(s))^T$.

Different representations of contours have been proposed in the literature (see e.g. [11] for an overview). The common denominator of these contour models is to represent $\mathcal{C}$ by as few parameters as possible while still meeting the requirements of the given application. The set of parameters needed to fully describe the contour at any instance in time is referred to as *state* of the model. Taking into account any evolution of the contour over time we can define the state-space representation of a contour by

$$\mathbf{x}_k = \mathbf{f}(\mathbf{x}_{k-1}, \mathbf{v}_{k-1}) \tag{3}$$

$$\mathbf{z}_k = \mathbf{h}(\mathbf{x}_k, \mathbf{w}_k), \tag{4}$$

where $\mathbf{f}(\cdot)$ represents the state transition of the state $\mathbf{x}$ from time $k-1$ to time k subjected to process noise which is modeled by $\mathbf{v}$. A measurement based on the current state $\mathbf{x}_k$ subjected to measurement noise $\mathbf{w}$ is modeled by $\mathbf{h}(\cdot)$. We are now able to formulate the reconstruction problem in the ECT as the problem of estimating the inner state (i.e. the current contour) of a dynamic system. In addition to approaches to reconstruct static setups, the use of dynamic models allows to extend the algorithm towards dynamically changing setups.

The different contour models have been designed in favor of distinct application requirements. In the sequel we will introduce the B-spline model and Fourier descriptors and their respective applicability to the ECT problem.

3.1. B-Spline Representation

Using splines as representation of contours requires to approximate the true contour $\mathcal{C}$ by a linear combination of spline functions. While we have some freedom in choosing different spline functions, a commonly used set of basis functions $b_n(s)$ are bicubic functions, where $n = 0, \ldots, (N-1)$ denotes the current index in a representation using N basis functions. The resultant model is referred to as *B-spline* representation of $\mathcal{C}$:

$$\hat{\mathbf{c}} = \begin{bmatrix} \mathbf{b}(s) & \mathbf{0} \\ \mathbf{0} & \mathbf{b}(s) \end{bmatrix} \begin{bmatrix} \mathbf{q}^x \\ \mathbf{q}^y \end{bmatrix} = U(s)\mathbf{q}. \tag{5}$$

The vectors $\mathbf{q}^x = (x_0, x_1, \ldots, x_{N-1})^T$ and $\mathbf{q}^y = (y_0, y_1, \ldots, y_{N-1})^T$ denote the coordinates of the N *control points* and are used as weights for the respective basis functions. The vector $\mathbf{b}(s)$ is given by $\mathbf{b}(s) = (b_0(s), b_1(s), \ldots, b_{N-1}(s))^T$. Thus, a B-spline is represented by a vector $\mathbf{q}$ of size $2N$. In order to reduce the number of required parameters we introduce the shape-space representation of B-splines [2]:

The shape space of a contour is given by a linear transformation that maps a shape-space vector $\mathbf{x}$ to a spline vector $\mathbf{q}$ such that

$$\mathbf{q} = W\mathbf{x} + \mathbf{q_0}, \tag{6}$$

where $\mathbf{q}_0$ represents a reference shape. Given that the dimension of the shape-space N_x is usually small compared to the size of the spline vector $N_q = 2N$, the shape-space representation results in a noticeable reduction of parameters. A B-spline now is represented by a reference B-spline $\mathbf{q}_0$ and a shape-space vector. The $N_x \times N_q$ shape-matrix W enforces that deviations from the reference spline are restricted to geometrically meaningful deformations. As an example, the affine transformation has 5 degrees of freedom (d.o.f.) and can be represented in shape-space via the following transformation:

$$\mathbf{q} = \begin{pmatrix} \mathbf{1} & \mathbf{0} & \mathbf{q}_0^x & \mathbf{0} & \mathbf{0} & \mathbf{q}_0^y \\ \mathbf{0} & \mathbf{1} & \mathbf{0} & \mathbf{q}_0^y & \mathbf{q}_0^x & \mathbf{0} \end{pmatrix} \mathbf{x} + \mathbf{q}_0, \tag{7}$$

where the reference shape vector $\mathbf{q}_0 = (\mathbf{q}_0^{xT}\mathbf{q}_0^{yT})^T$. Figure 2 depicts a reference spline and its possible geometric deformations based on an affine shape-matrix W as given by eqn. (7). Splines can be applied to problems where the reference contour $\mathbf{q}_0$ and its allowed geometric deformations are known. The restriction to a certain class of transformations in shape-space results in a high degree of regularization which can be utilized in the reconstruction process. In addition, splines lends themselves to model shapes stochastically by the introduction of random variables as elements within the shape-state vector $\mathbf{x}$. Figure 3(a) depicts a reference spline and $M = 5$ instances of this model given that the state vector is comprised Gaussian random variables. Splines fail to properly model shapes as soon as the current shape can not be represented within the given shape-space.

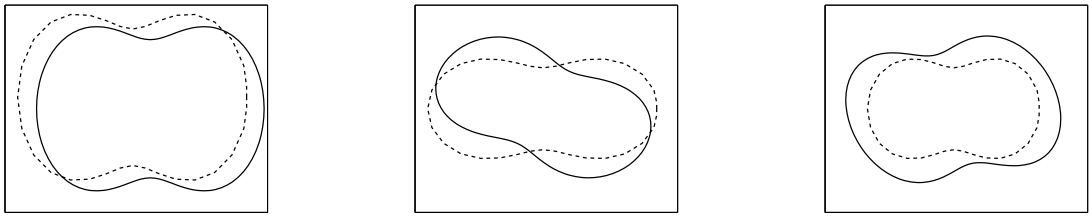

(a) (b) (c)

Figure 2: Geometric deformations of a B-spline subjected to an affine transformation (reference spline dashed): Pure translation (a), rotation (b), and scaling and shear (c).

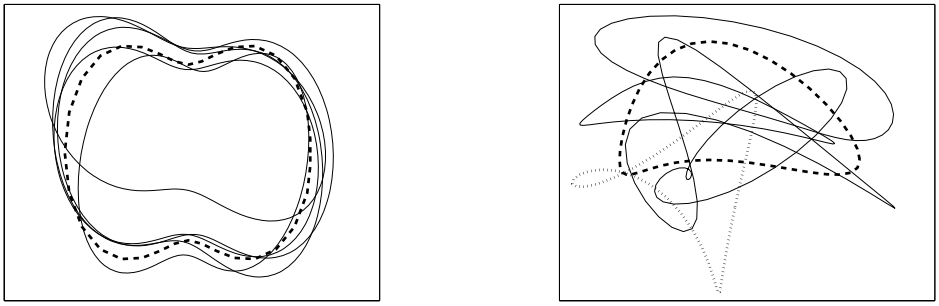

(a) (b)

Figure 3: Reference contours (dashed) and $M = 5$ random instances of the two contour models. (a) the B-spline representation is restricted to geometric deformations based on the shape-matrix. (b) varying the Fourier descriptors results in random contours not all of which have a physical meaning (see e.g. the dotted contour).

3.2. Fourier Descriptors

An alternative representation of a closed contour $\mathcal{C}$ is based on the property that for any closed contour the coordinate functions $x(s)$ and $y(s)$, respectively, are periodic with a period $T = 1$. Therefore, we can approximate both functions using the Fourier series expansions to obtain

$$\hat{x}(s) = \frac{a_{x,0}}{2} + \frac{1}{2\pi} \sum_{n=1}^{N-1} \left(a_{x,n} \cos(2\pi n s) + b_{x,n} \sin(2\pi n s) \right) \tag{8}$$

$$\hat{y}(s) = \frac{a_{y,0}}{2} + \frac{1}{2\pi} \sum_{n=1}^{N-1} \left(a_{y,n} \cos(2\pi n s) + b_{y,n} \sin(2\pi n s) \right). \tag{9}$$

The approximation improves as the number of coefficients in the series representation increases. In this context the Fourier series coefficients are referred to as *Fourier descriptors* of the contour.

As opposed to the B-spline representation state transitions of Fourier descriptors in general do not correspond to any restricted family of geometric transformations of the underlying shape. Thus, the geometric regularization is less stringent than it is for the B-spline model. However, using Parseval's theorem the magnitude of the Fourier descriptors $m_{x,i} = \sqrt{a_{x,i}^2 + b_{x,i}^2}$ can be interpreted as the energy of the contour in the given frequency band. This contour model can, therefore, be used to apply a frequency-dependent convergence criterion as low frequency components (i.e. the lower order Fourier descriptors) correspond to the coarse shape of the contour and high frequency components (i.e. the higher order Fourier descriptors) correspond to details of the contour. Figure 3(b) indicates the variations in shape as a consequence of a stochastic Fourier descriptor model. As opposed to the B-spline case the Fourier descriptors can result in loops which can not be used for the reconstruction of the objects under consideration in ECT.

4. PARTICLE FILTER

According to the Bayesian approach the estimate of the unknown inner state $\mathbf{x}_k$ of a dynamic system at any time k is based on the totality of information present up to time k which is available through the measurements $\mathbf{z}_i, i = 1, \ldots, k$. Whereas for the Kalman filter the state is modeled using a multi-variate Gaussian distribution, the PF numerically approximates the potentially multi-modal density of the state vector using the principle of *stochastic sampling*: a set of N points – the samples or particles $\mathbf{x}^{(m)}$ – randomly chosen from the state space and their respective weights $w^{(m)}$ can be used to represent a probability density function:

$$f_{\mathbf{x}}(\mathbf{x}) \approx \{\mathbf{x}^{(m)}, w^{(m)}\}_{m=1,\ldots,N} \tag{10}$$

This relation can be used to approximate moments of the true density such as the expected value. In this context, the dynamic model introduced in section 3 is reformulated using conditional densities: $p(\mathbf{x}_k|\mathbf{x}_{k-1})$ denotes the state transition density and $p(\mathbf{z}_k|\mathbf{x}_k)$ is used as measurement model. The PF keeps track of the current state estimate $p(\mathbf{x}_k|\mathbf{Z}_k)$, where $\mathbf{Z}_k = \{\mathbf{z}_1, \ldots, \mathbf{z}_k\}$ denotes the measurement history, in an iterative process.

Prediction: Prior to a measurement the state transition model is applied to predict the state $p(\mathbf{x}_k|\mathbf{Z}_{k-1})$ at time k using the Chapman-Kolmogorov equation

$$p(\mathbf{x}_k|\mathbf{Z}_{k-1}) = \int_{\Omega} p(\mathbf{x}_k|\mathbf{x}_{k-1}) p(\mathbf{x}_{k-1}|\mathbf{Z}_{k-1}) d\mathbf{x}_{k-1}. \tag{11}$$

Numerically the conditional density $p(\mathbf{x}_k|\mathbf{Z}_k)$ is represented using the sample set $S = \{\mathbf{x}_k^{(m)}, w_k^{(m)}\}$ where $m = 1, \ldots, N$. As indicated in Figure 4, the prediction step comprises a deterministic drift and a stochastic diffusion process. A number of important implementation details of the PF are hidden in the process of *resampling* required to ensure convergence and to control the size of the sample set. The reader is referred to introductory texts in [1, 3] and to van der Merwe et al. [10] for a discussion on different resampling strategies.

Measurement Update: The second step within the PF iteration uses the measurement model $p(\mathbf{z}_k|\mathbf{x}_k)$ to estimate the posterior density $p(\mathbf{x}_k|\mathbf{Z}_k)$ by applying Bayes' theorem:

$$p(\mathbf{x}_k|\mathbf{Z}_k) = \frac{p(\mathbf{z}_k|\mathbf{x}_k) p(\mathbf{x}_k|\mathbf{Z}_{k-1})}{p(\mathbf{Z}_k)} \tag{12}$$

The weights of the distinct samples in Figure 4 are denoted by their respective size. Note that for the measurement step no weights are taken into account. It is only during the measurement that the samples obtain new weights based on their amplification or attenuation by the measurement model.

The output of the PF algorithm is a set of samples which is used to approximate the posterior distribution. From these samples, any estimate of the system state such as expected value of the state

$$\hat{\mathbf{x}}_k = E\{\mathbf{x}_k|\mathbf{Z}_k\} \approx \sum_{m=1}^{N} w_k^{(m)} \mathbf{x}_k^{(m)} \tag{13}$$

can be calculated.

5. SIMULATION RESULTS

In order to verify the proposed state-space contour model approaches two different experiments of two-phase flow fields are performed. The simulations were carried out using a B-spline representation with a circular reference contour and a 6 d.o.f. shape-vector. For the Fourier descriptor approximation $2(2N + 1) = 10$ Fourier coefficients were used. The state transition (2) is assumed as a random walk process. The measurement process is modeled using

$$p(\mathbf{z}_k|\mathbf{x}_k) = \frac{1}{\sqrt{(2\pi)^n det(\mathbf{\Sigma})}} e^{-\frac{1}{2}(\mathbf{V_m}-\mathbf{V_c})^T \mathbf{\Sigma}^{-1} (\mathbf{V_m}-\mathbf{V_c})} \tag{14}$$

as likelihood function where $\mathbf{V}_c$ denotes the estimated and $\mathbf{V}_m$ the measured electrode potentials. The Gaussian nature of the measurement noise has been validated by an analysis of $M = 2000$ Monte Carlo trials. During these simulations the underlying covariance matrix $\mathbf{\Sigma}$ has been estimated. The first test case illustrates the convergence behavior of the applied PF when the spline representation is used to describe the boundaries of a gas bubble ($\varepsilon_r = 1$) in oil ($\varepsilon_r = 2$). The PF is initialized with 16 particles of circular shape that are uniformly distributed over the cross-section of the pipe. The reference object, i.e. the water bubble to be located, has an elliptical form.

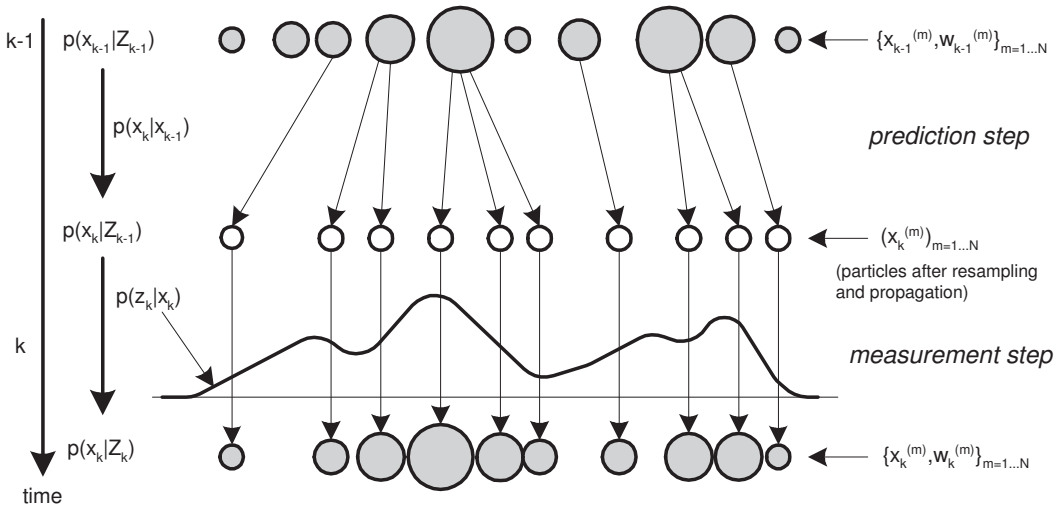

Figure 4: Principle of particle filtering. The old sample set at $k-1$ approximates the previous state density $p(\mathbf{x}_{k-1}|\mathbf{Z}_{k-1})$. The sizes of the particles reflect their weights that are assigned to them. After resampling and propagation through the state model, all particles have the same weights. However, samples with small weights have been removed, while samples with large weights have been replicated. In the measurement step, the measurement model $p(\mathbf{z}_k|\mathbf{x}_k)$ assigns new weights to each sample.

It is indicated as bold dashed contour in Figure 5. The grey contours show the single particles, while the bold black object stems from the expectation of the posterior state density. The situation after the second iteration of the PF is depicted in Figure 5(a), while Figure 5(b) points the state after iteration 4. After only four iterations almost all particles are contracted to the right position. However, the size and the shape still have to be adjusted. The estimation result after 25 iterations is plotted in Figure 6(a). There are still particles with wrong position, size and shape originating from the stochastic sampling, but the associated weights of these particles are low. The expectation of the state density approximates the true bubble reasonably well. The progression of the estimated center is illustrated in Figure 6(b). It can be seen that after about 5 iterations the estimate for the center is within a tolerance band where it remains over the iterations.

The second experiment consists of a gas bubble resembling a triangle in oil, shown as bold dashed contour in Figure 7. Such a shape cannot be emulated with splines based on an affine transformation of a circular reference shape, as used in our work. However, the true shape of the bubble can be exactly matched with second order Fourier descriptors. The performance of the PF with spline-based contour model is illustrated in Figure 7, where

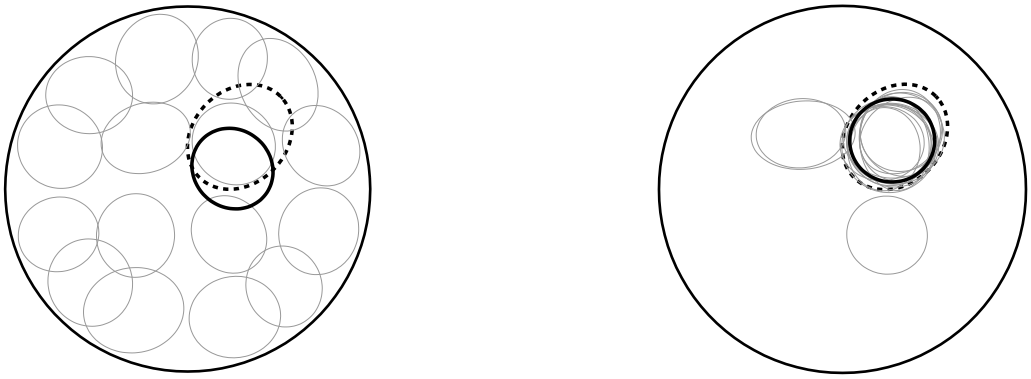

(a) Iteration 2.

(b) Iteration 4.

Figure 5: Evolution of the PF with B-spline contour model for a gas bubble immersed in oil. The plots show all particles (thin grey contours) and the expectation of the posterior state density (bold black contour) in comparison with the true bubble (bold dashed contour) after iterations 2 and 4, respectively.

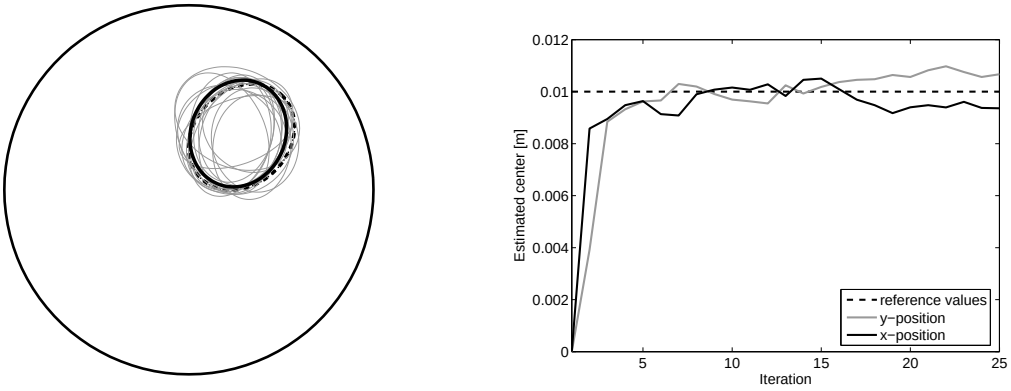

(a) Iteration 25.

(b) Estimated center of the bubble.

Figure 6: Estimation result of the PF with B-spline contour representation after 25 iterations. The estimated shape (bold line) is almost congruent with the reference shape (dashed line). The chart on the right illustrates the progression of the estimated center coordinates where the dashed line corresponds to the reference position ($x = y = 0.01$m). The center of the pipe is the point of origin.

the expectation of the posterior distribution at different iterations is compared with the true bubble. The filter is initialized with 30 particles to perform a deeper sampling of the true object shape. The filter estimates after 2, 16 and 30 iterations are shown in the figure. Similar to the first example shown in Figure 5 the true object position can be reached after a few filter iterations, while a reasonable approximation of the reference shape takes more iterations. The estimate of iteration 30 is depicted in Figure 7(c), where the shape of the spline contour is an ellipsoidal approximation of the true bubble. A better match is not achievable with the used contour model. However, the filter with B-spline model is able to produce robust approximations of complex contours due to the low number of hidden states. The performance of the PF with a second order Fourier descriptor shape model on

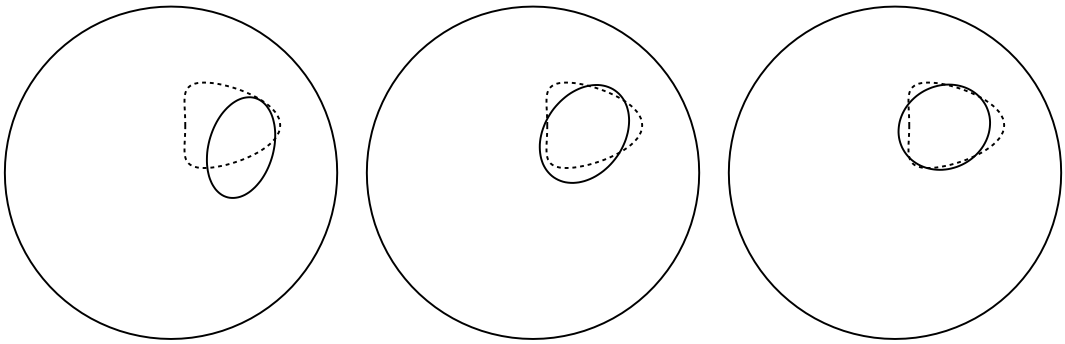

(a) Iteration 2.

(b) Iteration 16.

(c) Iteration 30.

Figure 7: Contour estimates of the PF with B-spline contour model for a triangle-like gas bubble at different iterations. The dashed contour indicates the true bubble shape. The used model does not allow an exact match the true shape.

the same reconstruction problem is illustrated in Figure 8. The evolution of the shape estimates is very similar to that of the spline-based filter. In contrary to the spline model, the Fourier descriptor model is in principle capable of exactly matching the reference contour. However, the ECT problem is ill-posed, i.e. the sensitivity of the measured electrode potentials with respect to higher-order contour details is very poor. Therefore the power of the Fourier descriptor model cannot be exploited in the present application. As can be seen from Figure 8(c), the shape reconstruction is qualitatively similar to the spline-based results.

To further study the correlation between the sensitivity of the forward problem and the reconstruction quality, the PF with Fourier descriptors is applied to a third test case. The reference bubble is a triangle with sharp edges and a dent on one side. The edges cannot be reconstructed if a gas bubble with a relative permittivity $\varepsilon_r = 1$ is assumed. However, in the performed experiment the bubble is assumed to consist of water with $\varepsilon_r = 80$. This results in a stronger contrast between the bubble and the background medium and therefore in a higher sensitivity

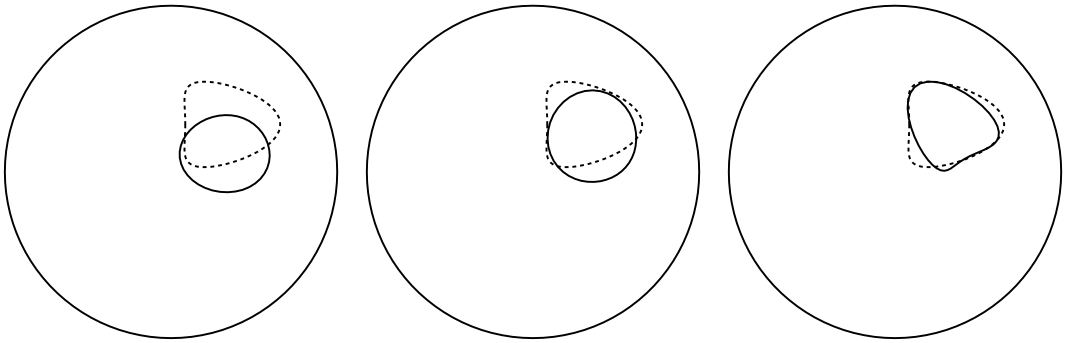

(a) Iteration 2. (b) Iteration 16. (c) Iteration 30.

Figure 8: Contour estimates of the PF with Fourier coefficient contour model for a triangle-like gas bubble at different iterations. The dashed contour indicates the true bubble shape. The used model would allow to exactly match the true shape, but it cannot be achieved due to the ill-posedness of the problem.

of the forward problem to fine details in the problem region. The filter performance is illustrated in Figure 9. The edges and the straight lines of the reference contour can be matched much better than for gas bubbles due to the higher sensitivity of the forward problem.

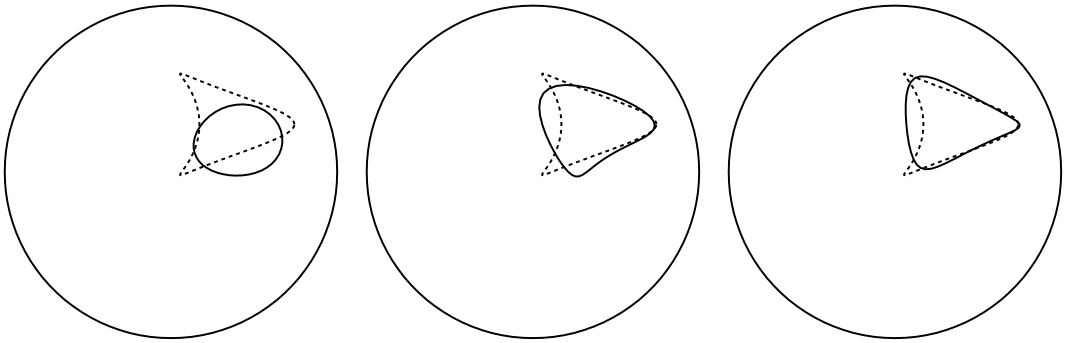

(a) Iteration 2. (b) Iteration 20. (c) Iteration 40.

Figure 9: Contour estimates of the PF with Fourier coefficient contour model for a triangle-like water bubble with sharp edges at different iterations. The dashed contour indicates the true bubble shape. Due to the high permittivity contrast between water and oil the details of the true contour can be better matched than for gas bubbles.

6. CONCLUDING REMARKS

In this contribution a novel approach to describe closed contours in the state-space for two-phase fields in ECT is proposed. The boundary of the object to be located, is modelled by a parameterized curve. Two different approaches, a description with B-splines and a Fourier representation are investigated and compared. In order to take measurement uncertainties into account, the inverse problem is recast in form of statistical inference and solved by means of particle filtering. A kind of regularization is implicitly achieved which can be directly interpreted in the object domain as it relates to smooth contours. With B-spline representation with the affine model the object position and the fundamental component of the shape can be reconstructed reasonably well. In general, Fourier descriptors are able to model more complex contours. In fact, due to the poor sensitivity of the forward problem in case of oil-gas flow, only results comparable to B-splines are achievable. However, for problems with higher sensitivity, e.g. oil-water flow, even higher order components of the object can be resolved with Fourier descriptors.

REFERENCES

1. M. S. Arulampalam, S. Maskell, N. J. Gordon and T. Clapp, A tutorial on particle filters for online nonlinear/non-Gaussian Bayesian tracking, *IEEE Trans. on Signal Processing*, (2002), **50**(2), 174-188.

2. A. Blake and M. Isard, *Active Contours*, Springer-Verlag, Berlin, 1998.

3. A. Doucet, N. de Freitas and N. J. Gordon, *Sequential Monte Carlo Methods in Practice*, Springer-Verlag, New York, 2001.

4. P.C. Hansen, *Rank-Deficient and Discrete Ill-Posed Problems*, Society for Industrial and Applied Mathematics (SIAM), Philadelphia, 1998.

5. J. P. Kaipio, V. Kolehmainen, E. Somersalo and M. Vauhkonen, Statistical inversion and Monte Carlo sampling methods in electrical impedance tomography, *Inverse Problems*, (2000), **16**(5), 1487-1522.

6. K.Y. Kim, B.S. Kim, M.C. Kim, S. Kim, Y.J. Lee, H.J. Jeon, B.Y. Choi and M. Vauhkonen, Electrical impedance imaging of two-phase fields with an adaptive mesh grouping scheme. *IEEE Trans. on Magnetics*, (2004), **40**(2), 1124-1127.

7. P. Charbonnier, L. Blanc-F$\acute{e}$raud, G. Aubert and M. Barlaud, Deterministic edge-preserving regularization in computed imaging, *IEEE Trans. on Image Processing*, (1997), **6**(2), 298-311.

8. B. Kortschak and B. Brandstätter, A FEM-BEM approach using level-sets in tomography, *Proceedings of the 11th Int. IGTE Symposium on Numerical Field Calculation in Electrical Engineering*, Graz-Seggauberg, Austria, 2004, pp. 301-307.

9. T. Martin and J. Idier, A FEM-based nonlinear MAP estimator in electrical impedance tomography, *Proceedings of the Int. Conference on Image Processing*, **2**, 1998, pp. 684-687.

10. R. van der Merwe, A. Doucet, N. de Freitas and E. Wan, The unscented particle filter, *Technical Report CUED/F-INFENG/TR 380*, Cambridge University Engineering Department, August 16, 2000.

11. M. Sonka, V. Hlavac, R. Boyle, *Image Processing, Analysis, and Machine Vision*, 2nd edition, Brooks/Cole Publishing Company, 1999.

12. M. Vauhkonen, P. A. Karjalainen and J. P. Kaipio, A Kalman filter approach to track fast impedance changes in electrical impedance tomography, *IEEE Trans. on Biomedical Engineering*, (1998), **45**(4), 486-493.

13. D. Watzenig, G. Steiner and B. Brandstätter, Managing noisy measurement data by means of statistical parameter estimation in electrical capacitance tomography, *Proceedings of the 11th Int. IGTE Symposium on Numerical Field Calculation in Electrical Engineering*, Graz-Seggauberg, 2004, pp. 196-201.

14. R. A. Williams and M. S. Beck, *Process Tomography, Principles, Techniques and Applications*, Butterworth-Heinemann Ltd., Oxford, 1995.